Numerical Methods in Civil Engineering, 10-4 (2026) 12-29

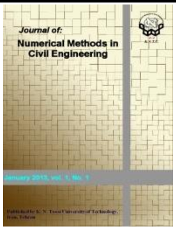

Numerical Methods in Civil Engineering

Journal Homepage: https://nmce.kntu.ac.ir/

Numerical Investigation of the Effect of CFRP Sheet Angle and Arrangement on the Shear Capacity of Reinforced Concrete Deep Beams

Alireza Abbaszadeh*, Taleb Hashminezhad**

ARTICLE INFO

RESEARCH PAPER

Article history:
Received:
February 2026
Revised:
May 2026
Accepted:
August 2026

Keywords:
Reinforced Concrete
Deep Beam
CFRP
Shear Strengthened
Finite Element Method

Abstract:

Deep beams generally suffer from limited shear capacity and ductility due to their specific aspect ratio and the significant contribution of shear deformation to their overall response. Consequently, various methods have been employed to strengthen these structural members. Among these, reinforcing the beam web with Carbon Fiber Reinforced Polymer (CFRP) sheets is considered one of the most effective solutions. Given the inherent limitations of conventional steel reinforcement in significantly enhancing shear capacity and ultimate strength, CFRP sheets have emerged as an effective alternative and are currently the focus of extensive research.

In this study, the shear behavior of CFRP-strengthened deep beams is investigated using numerical simulation in the ABAQUS finite element software. To this end, sixteen deep beam specimens with constant longitudinal reinforcement but varying shear span-to-depth ratios (a/d) were designed and analyzed under two concentrated loads equidistant from the supports. From this set, four models served as control specimens (un-strengthened), and the remaining twelve models were strengthened in the shear zone using CFRP sheets.

The results indicated that the maximum shear contribution of CFRP is achieved with a 135 degree orientation, particularly in beams exhibiting shear-dominant behavior (low a/d ratio). Specifically, an increase in ultimate capacity up to 50% was observed, along with a reduction in rebar stress compared to the strengthened state.

1. Introduction

Reinforced concrete (RC) deep beams serve as primary load-bearing elements in various structures, such as shear walls, transfer girders in large-span structures, and even shear cores. They play a crucial role in the direct transfer of vertical forces and in resisting high shear loads. The distinguishing characteristic of these beams is their low shear span-to-effective depth ratio (typically less than 2.5), which results in shear-dominant behavior and complex load transfer mechanisms that differ from those of conventional beams [1]. This behavior makes them highly vulnerable to shear failure, which is often characterized as brittle and exhibits minimal ductility [2].

Recent studies have further explored this topic using advanced numerical methods. For instance, Abadel et al. [3] investigated RC deep beams strengthened in shear using NSM-CFRP bars with ABAQUS, reporting shear capacity enhancements of 18.3–151.3% and a maximum 10% error between experimental and numerical results. Similarly, Kumar and Jangid emphasized the lack of design guidelines for CFRP-strengthened deep beams, a gap that the present study partially addresses[4].

The inherent shear weakness of deep beams has driven researchers toward developing various strengthened solutions. Conventional methods, such as the use of steel shear reinforcement (stirrups), although being effective, face several limitations, including physical space occupation, difficulty of implementation, and corrosion potential, and their capacity to increase resistance is asymptotically limited [5]. Over the last two decades, the use of Fiber Reinforced Polymer (FRP) composites has gained widespread acceptance as a novel and efficient alternative for strengthening concrete structures [6]. These materials, due to advantages such as exceptionally high strength, light weight, corrosion resistance, and ease

* *Corresponding author: Assistant Professor, Department of Civil Engineering, Ilam University, Ilam, Iran. Email: a.abaszadeh@Ilam.ac.ir*
** *Graduated civil Engineering, Razi University, Kermanshah, Iran.*

https://doi.org/10.61882/NMCE.2602.1131

of installation, have established a new paradigm in structural rehabilitation and repair [7].

Among the types of FRPs, CFRP (Carbon Fiber Reinforced Polymer) sheets have found the most widespread application in beam shear strengthening due to their highly desirable tensile strength and modulus of elasticity [8]. The action mechanism of these sheets is similar to that of stirrups: they resist tensile forces in the shear zone, consequently increasing the overall beam capacity. Numerous experimental and numerical studies have investigated this topic. For instance, research by Abadel et al. (2022) and Akkaya et al. (2022) has shown that CFRP shear strengthening can increase the ultimate load-bearing capacity of deep beams by up to 60% [9] [10] . Furthermore, a numerical study conducted using the ABAQUS software by Li et al. confirmed that this method not only improves strength but also enhances the buckling behavior of the beam [11].

Despite the remarkable progress in the field of shear strengthening of RC deep beams using Carbon Fiber Reinforced Polymer (CFRP) composites, the influence of the key parameter of the shear span-to-effective depth ratio (a/d) on the load transfer mechanism and shear behavior of these members has not been comprehensively and systematically investigated [12].

To address this research gap, the shear behavior of RC deep beams deficient in shear reinforcement (i.e., those that do not satisfy the minimum shear reinforcement requirements stipulated by design codes) was investigated using accurate numerical simulation in ABAQUS software. The main focus of this study was to evaluate the efficiency of CFRP strengthening sheets with various arrangements and angles under different (a/d) ratios.

The main novelty (or primary contribution) of this research lies in the simultaneous and systematic investigation of the influence of two key parameters the angle and arrangement of the CFRP sheets and the shear span-to-depth ratio (a/d) on the shear capacity and failure behavior of deep beams. This combined systematic effect has not been comprehensively addressed in prior studies.

Background and Theoretical Framework

The structural behavior of Reinforced Concrete (RC) deep beams is distinct from that of conventional beams due to their small span-to-depth ratio. In deep beams, the assumption of linear stress distribution over the section depth is not valid, and a significant portion of the load is transferred through arch-shaped compression paths. Therefore, their analysis requires consideration of the stress field mechanism, typically modeled using the Strut-and-Tie Model [13] [14]. In this model, the compression zones are idealized as compression elements (struts), and the longitudinal or shear reinforcements are idealized as tension members (ties), which collectively form the load transfer path from the loading points to the supports.

In deep beams, a significant proportion of the total deformations is attributed to shear deformations, and diagonal cracks within the load transfer regions commonly lead to sudden and brittle failure [15]. Therefore, enhancing shear capacity by strengthening the critical web areas is of particular importance. The use of CFRP sheets as a high-modulus and lightweight material is considered an effective method for improving shear resistance. The mechanism of CFRP action in deep beams is based on resisting the tensile forces generated by shear and restricting the propagation of diagonal cracks [16]. Essentially, CFRP acts similarly to steel stirrups, preventing the sudden widening of shear cracks and thus changing the failure mode from brittle to ductile [17].

The arrangement of the CFRP sheets on the beam web surface has a significant impact on shear performance. Studies have indicated that the diagonal orientation of the fibers relative to the beam axis (typically at a 135 degree angle) provides the most effective contribution to resisting shear forces [18]. Furthermore, increasing the sheet thickness and improving the bond strength between the CFRP and the concrete through proper surface preparation considerably enhances the ultimate capacity [19].

Researchers in numerous studies have investigated the effect of shear strengthened with CFRP composites in deep beams. In experimental studies, results have indicated that the use of CFRP leads to an increase of 40% to 60% in the ultimate load-bearing capacity compared to unstrengthened beams [20]. Chen et al. reported that CFRP sheets with diagonal arrangements, while increasing shear capacity, also result in a reduction in crack widths and a delay in failure [21].

Rahmani et al., in an experimental study, found that the shape and bonding pattern of the CFRP directly affect the shear resistance, noting that the U-shaped scheme is more effective in deep beams. Conversely, Kim et al., using numerical modeling in ABAQUS software, demonstrated that as the shear span-to-depth ratio (a/d) increases, the shear contribution to the overall behavior decreases, and the effectiveness of the CFRP is subsequently limited [21]. Some other studies have investigated the debonding of CFRP from the concrete surface, which is considered one of the main challenges of this strengthened method [22]. Zhang et al. further studied the effects of dynamic loads on FRP sheet debonding and proposed relevant equations for this failure mode [23].

In another study, the structural behavior of deep reinforced concrete beams with large beam web openings reinforced with fibers, bamboo and steel sheets was studied[24], [25], [26].

The synthesis of past research indicates that while the positive effect of CFRP on the shear capacity and ductility of deep beams has been proven, a comprehensive investigation into the influence of the shear span-to-depth ratio (a/d) on the efficiency of the strengthened system and the failure behavior remains an open topic requiring further research. To address this gap, the present study was conducted to numerically simulate the behavior of CFRP-strengthened deep beams under various (a/d) ratios using ABAQUS software.

Unlike previous studies that examined CFRP orientation and a/d ratio independently, this research simultaneously and systematically investigates both parameters. The novelty lies in the combined evaluation of three CFRP angles (45°, 90°, 135°) across four different a/d ratios (0.95 to 1.35) in deep beams that are intentionally deficient in shear reinforcement a parametric combination not previously addressed in the literature.

2. Methodology

2.1 Numerical modeling

In this research, the shear behavior of Reinforced Concrete (RC) deep beams with and without CFRP shear strengthening was numerically modeled and investigated using the ABAQUS finite element software. The main objective of this study is to examine the effects of the key parameter, the shear span-to-depth ratio (a/d), as well as the presence or absence of CFRP, on the ultimate capacity and crack pattern of the beams. To this end, a set of three-dimensional (3D) deep beam models with identical geometric specifications but varying (a/d) ratios was simulated.

In the present numerical models, a perfect bond is assumed between CFRP sheets and the concrete surface, meaning that no relative slip or debonding occurs at the interface. It is acknowledged that debonding represents a common failure mode in CFRP-strengthened RC members and may lead to an overestimation of ultimate capacity under the perfect bond assumption. However, this simplification is considered acceptable for the primary purpose of this study, such as comparative parametric evaluation of CFRP orientation and a/d ratio effects. The quantitative results should therefore be interpreted with due consideration of this limitation.

All strengthened and unstrengthened deep reinforced concrete beams in this study were selected with identical lengths, cross-sectional dimensions, flexural and shear reinforcement amounts, with the sole differences lying in the extent and type of strengthening as well as the positioning of concentrated loads. Another noteworthy point is that the web strengthened amount remains consistent across each specific strengthened model type, yet varies among models employing different configurations. This standardized approach ensures controlled variables for reliable comparative analysis in structural performance evaluation.

The arrangement of reinforcement bars used in the beam cross-section is illustrated in Figure 1. The tension rebar is 4Ø16 allocated at the bottom of the section. These bars are placed in two layers; to provide the necessary anchorage, the bars are passed through holes in a 10 mm thick steel end plate at their ends and welded around the bar circumference to the exterior side of the end plate.The shear reinforcements, with a diameter of 6 mm, are spaced at 150 mm intervals both horizontally and vertically. This quantity of shear reinforcement does not satisfy the minimum requirements stipulated in Iran's Chapter 9 Regulations or the ACI standards; therefore, all studied beams exhibit structural deficiency in shear.

All beams have dimensions of 1500 mm length, 120 mm width, and 500 mm height; to prevent concrete crushing, 20 mm thick and 100 mm long steel plates spanning the full beam width are employed at concentrated load points and supports. Supports are the simple type with symmetric concentrated loading. Loading consists of two concentrated forces applied at equal distances from the supports to create four-point bending conditions. At beam ends, boundary conditions incorporate one simple support and one roller support to avoid additional restraints.

3. Property of materials

In this study, concrete was simulated using the Concrete Damaged Plasticity model in ABAQUS. The mechanical properties of the concrete used in the beams include a characteristic compressive strength of 30 MPa, specific weight of 2400 kg/m³, and modulus of elasticity of 25743 MPa.

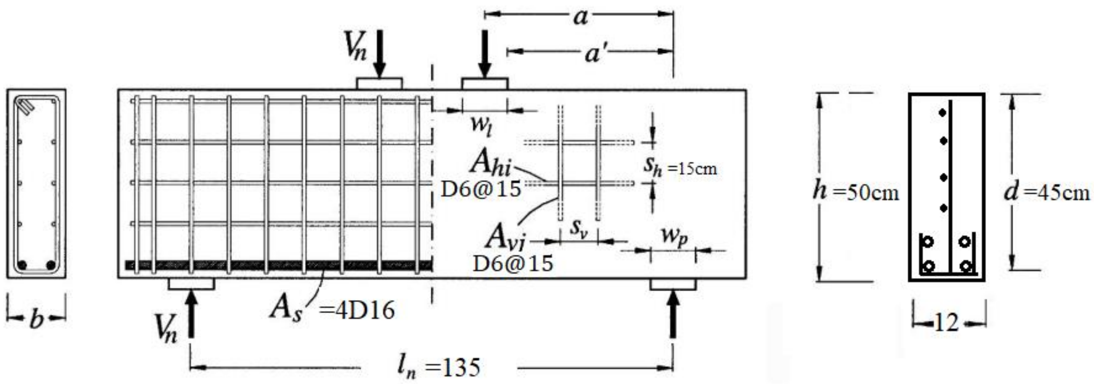

Fig. 1: Configuration of main reinforcement, horizontal and vertical reinforcements

Considering the compressive and tensile behavior of concrete, as illustrated in Figures 2, unloading from any point on the softening branch of the stress-strain curve results in a reduction of the material's elastic stiffness. This reduction in elastic stiffness is a function of temperature, field variables, and plastic strains, and is expressed through parameters that correspond d_t , d_c respectively to compression and tension.

$$d_c = d_c(\tilde{\varepsilon}_c^{pl}, \theta, f_i), \quad 0 \le d_c \le 1$$
$$d_t = d_t(\tilde{\varepsilon}_t^{pl}, \theta, f_i), \quad 0 \le d_t \le 1 \quad (1)$$

A damage parameter value of zero indicates no material damage, while a value of one signifies complete loss of strength. By introducing user-defined damage parameters (d_t و d_c) to the ABAQUS software, these parameters are automatically applied by the software itself in the calculations for elastic stiffness reduction during the unloading branch.

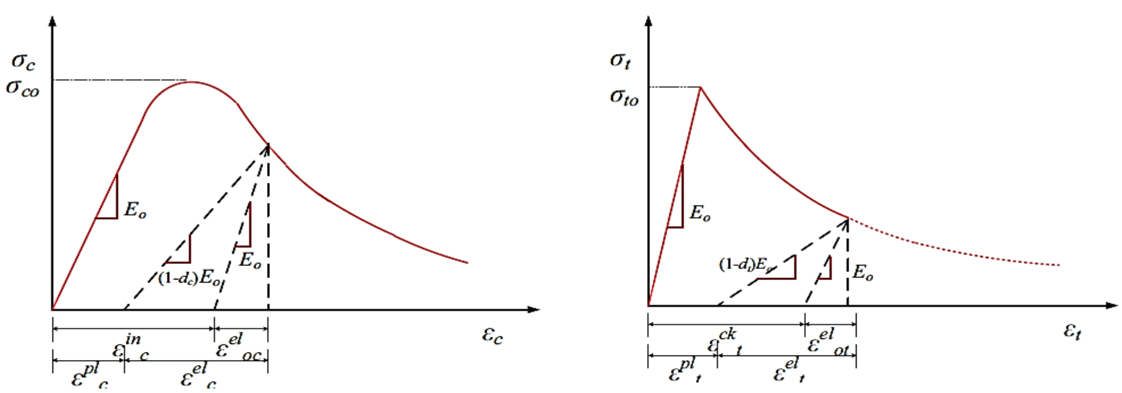

Fig. 2: Effect of damage parameters on concrete stiffness. (a) In tension (b) In compression[27]

The concrete damage variables were derived from the studies by Sumer and Ektas. As shown in the figure, the reduced elastic stiffness is obtained by multiplying the initial elastic modulus of undamaged concrete by $(1-d_c)$in compression and $(1-d_t)$ in tension.

$$\begin{cases} E_c = (1-d_c)E_0 \\ E_t = (1-d_t)E_0 \end{cases} \quad (2)$$

Tensile and compressive stresses can be expressed by ε^{in} as functions of inelastic strains, rather than plastic strains ε^{pl}. The inelastic strain is obtained as the difference between the total strain and the elastic strain of undamaged concrete, according to the following relations.

$$\varepsilon^{in} = \varepsilon - \varepsilon_0^{el} \quad (3)$$

$$\varepsilon_0^{el} = \frac{\sigma}{E_0} \quad (4)$$

The inelastic strains, ε^{pl} and ε^{in} along with the damage parameters, dc and dt, are introduced to the ABAQUS software for both tension and compression. ABAQUS then converts the inelastic strain values to plastic strain values using the following relationship.

$$\varepsilon^{pl} = \varepsilon^{in} - \frac{d}{(1-d)}\frac{\sigma}{E_0} \quad (5)$$

Damage parameters in confined concrete depend not only on inelastic strain but also on confinement pressure [27].

Truss elements (T3D3) were employed for modeling the reinforcement bars. This three-dimensional truss element features two nodes, each with three translational degrees of freedom, and exhibits both compressive and tensile strength along the member's axis. These elements were integrated with the concrete through the Embedded Region constraint.

CFRP sheets were defined as shell elements with a thickness of 1.2 mm on the beam web regions, using different patterns (vertical and 45° diagonal). Carbon fiber properties included an elastic modulus of 230 GPa, ultimate tensile strength of 4000 MPa, and Poisson's ratio of 0.25; the epoxy adhesive between concrete and CFRP was assumed to provide perfect bonding. However, it should be emphasized that this perfect bond assumption (implemented via a tie constraint in ABAQUS) does not account for potential interfacial debonding between the CFRP sheet and the concrete substrate. In shear-critical deep beams — particularly those with low a/d ratios — high interfacial shear stresses may develop, which can trigger premature debonding failure. Therefore, the current modeling approach provides an upper-bound estimate of the strengthening efficacy. Future refinements using cohesive zone models (e.g., surface-based cohesive behavior or cohesive elements) are necessary to capture bond-slip behavior more realistically.

FRP materials exhibit elastic-brittle behavior where damage initiates without significant deformation, thus plasticity is generally not considered in their modeling, and the Hashin failure criterion was employed for FRP simulation. Given FRP material properties, meshing utilized Quad-shaped shell elements from the S4R family.

4. Verification of Model

We apply the FE method using ABAQUS software in order to simulate the models. For the concrete components, three-dimensional 8-node reduced-integration solid elements (C3D8R). In a convergence study of FE models, reducing the element size is expected to improve the accuracy of the calculations. In this study, the convergence of the FE models is shown in Fig. 3-a, which reveals a decrease in the analysis error against the number of elements.

To validate the numerical modeling approach, the finite element results were compared with experimental data from previously tested deep beams available in the literature [28]. Figure 4 presents a comparison of the load–midspan displacement curves from the FE analysis and the experiment.

The FE model predicts an ultimate load of 351 kN, while the experimental value is 342 kN, a difference of 2.6%. The displacement at ultimate load is 20 mm from FE versus 18.7 mm from the experiment (6.9% difference). These small discrepancies are acceptable for parametric studies.

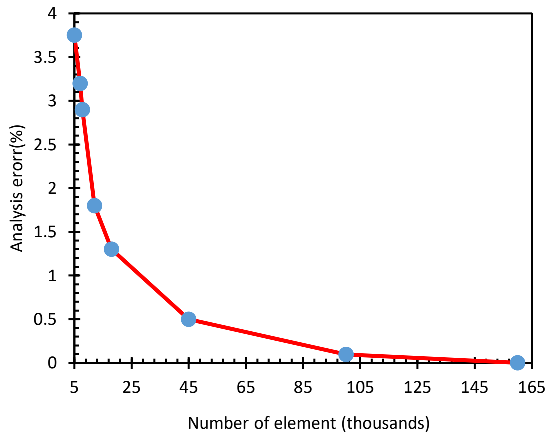

(a)

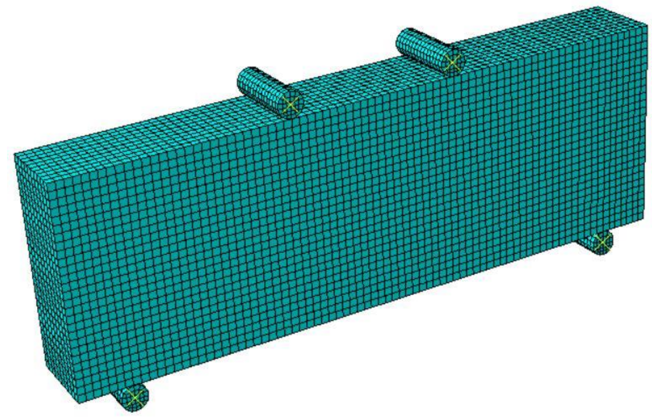

(b)

Fig. 3: a) analysis error percentage with number of elements b) Schematic of meshing model

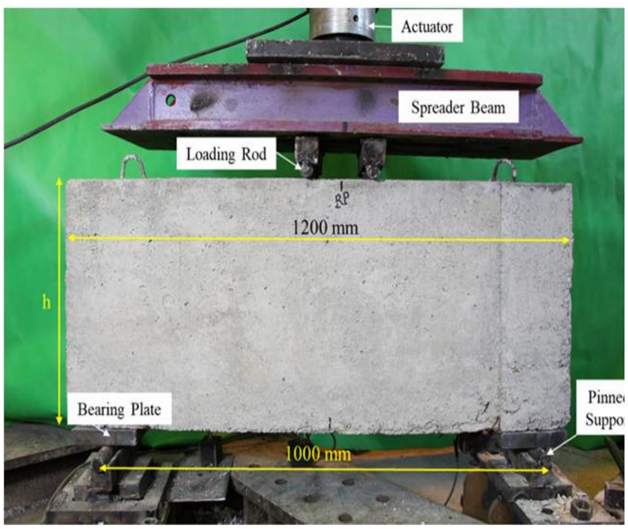

(a)

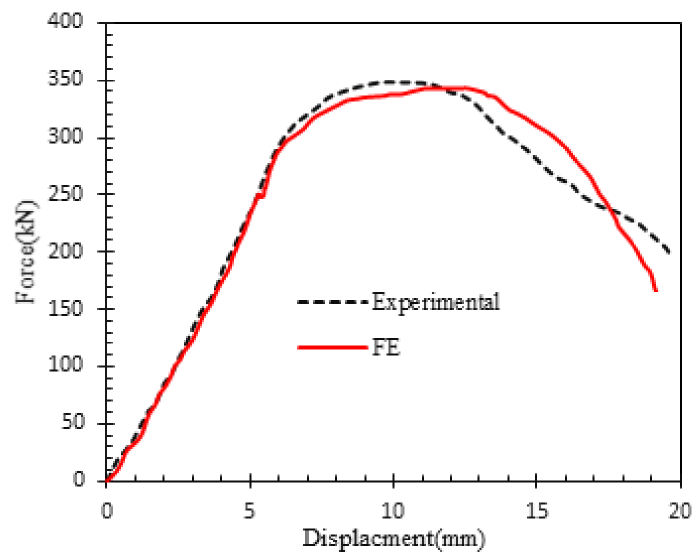

(b)

Fig. 4: load- displacement and Experimental model: a) Experimental model, b) Load –Displacement [28]

Table 1 summarizes the comparison. The close agreement in load, displacement, and failure mode supports the reliability of this numerical approach for comparative parametric analysis of CFRP orientation and a/d ratio effects.

Table 1: summarizes the comparison of FE and Experimental[28]

Parameter	Experiment	Present FE	Difference
Ultimate load (kN)	342	351	2.6%
Displacement at ultimate (mm)	18.7	20	6.9%
Failure mode	Diagonal shear	Diagonal shear	✓ Compatible

5. Meshing of Models

To achieve a precise analysis of the models, different mesh densities were employed in the critical region. The meshing strategy adopted for the models is illustrated in Figure 5. For the concrete components, three-dimensional 8-node reduced-integration solid elements (C3D8R) with a characteristic mesh size of 20 mm were utilized in the critical zone. This three-dimensional element belongs to the family of continuum stress-strain elements, featuring 8 nodes per element with three translational degrees of freedom at each node.

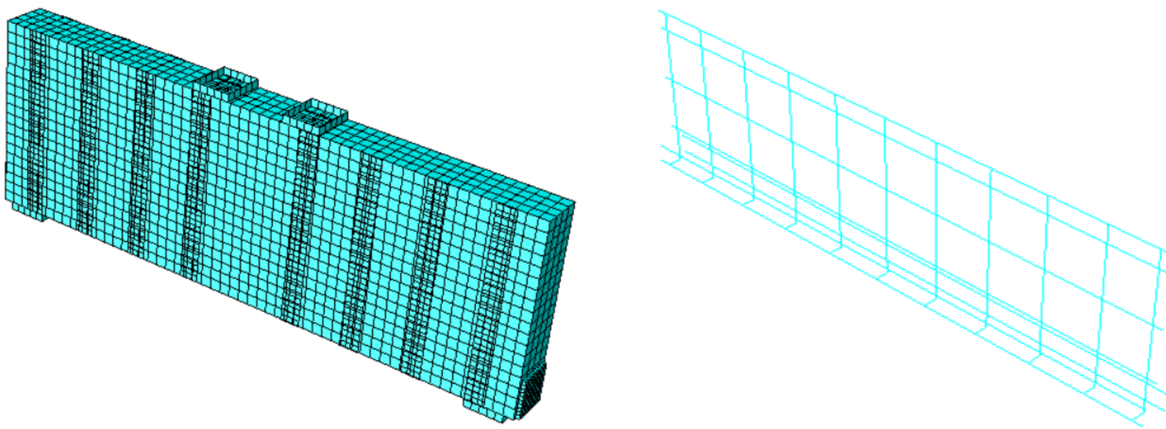

Fig. 5: Finite element meshing of the analyzed models

The element enables placement of reinforcement bars with varying properties in three arbitrary directions and is suitable for structures with or without reinforcing bars. The analysis type employed was nonlinear static analysis, which facilitates tracking of structural behavior up to ultimate failure.

6. Introduction to Simulated Models

In this study, a single type of reinforcing material was used: CFRP sheets. The CFRP thickness was 1.2 mm, while the sheet width varied depending on the orientation angle. The widths investigated were 18, 24, and 30 cm. For the five-layer CFRP configuration, the width of each strip was 5 cm, and the spacing between strips was adjusted according to the orientation angle.
To introduce the models, the expression C-a-b-c-d is used, where a is the number of reinforcement strips, b is the orientation angle of the sheets, c is the width of the sheet, and d is the shear span-to-depth ratio of the beam. For example, C-1-135-18-0.95 represents a model with one reinforcement strip, an orientation angle of 135 degrees, a sheet width of 18 centimeters, and an a/d ratio of 0.95. The specifications of 16 models examined are presented in the table below.

Table 2: Description of the Studied Models

model	**Orientation spacing cm**	**Orientation angle**	**Additional web strength ratio**	**Schematic Model**
C-0-0-0-0.95	_	-	_	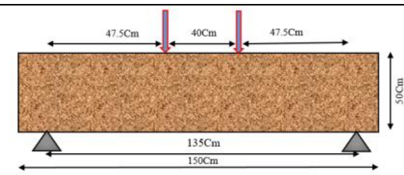
C-0-0-0-1.1	_	-	-	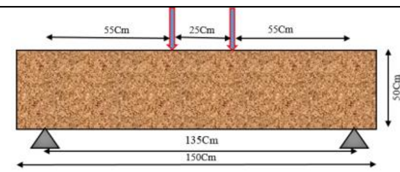
C-0-0-0-1.2	-	-	-	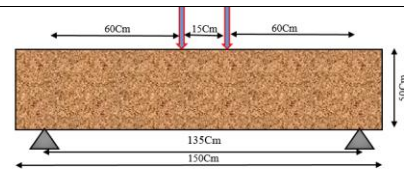
C-0-0-0-1.35	-	-	-	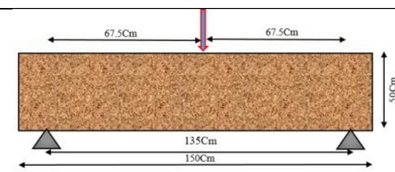
C-1-45-18-0.95	-	45	0.11	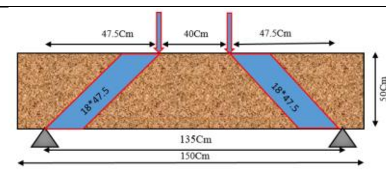
C-1-45-18-1.1	-	45	0.11	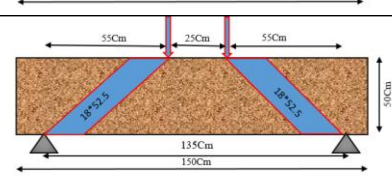
C-1-45-24-1.2	-	45	0.11	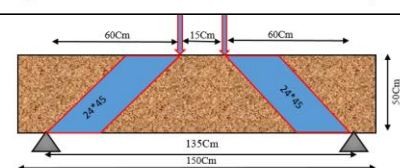
C-1-45-30-1.35	-	45	0.11	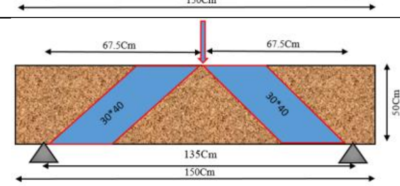

C-5-135-5-0.95	5	135	0.6	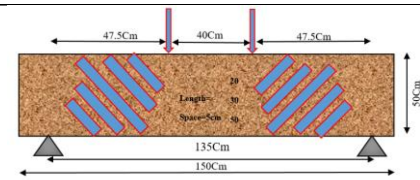
C-5-135-5-1.1	5	135	0.6	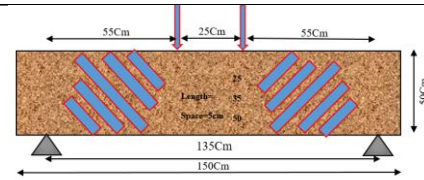
C-5-135-5-1.2	5	135	0.6	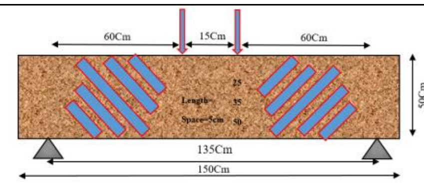
C-5-135-5-1.35	4	135	0.6	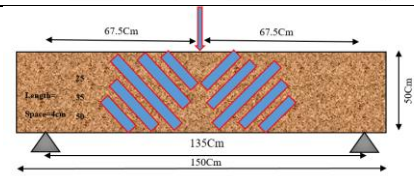
C-4-90-5-0.95	10	90	0.7	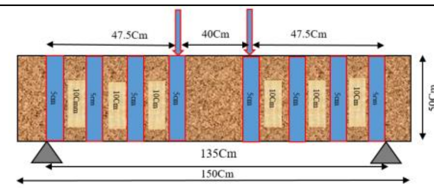
C-4-90-5-1.1	11.66	90	0.7	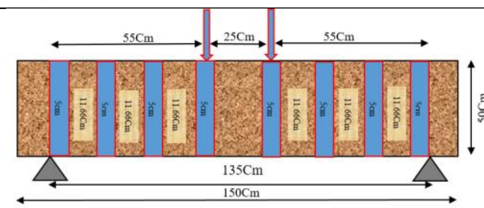
C-4-90-5-1.2	12.66	90	0.7	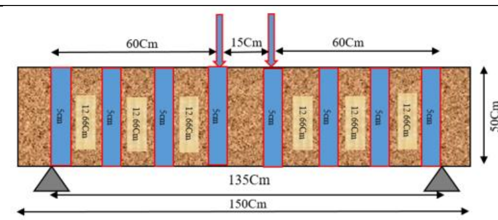
C-4-90-5-1.35	10.625	90	0.7	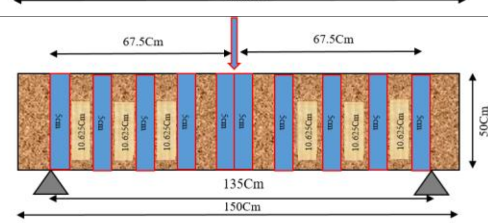

The results of each model, including the load–displacement curve, principal stress distribution, crack pattern, and ultimate capacity, were obtained and compared. crack pattern, and ultimate capacity, were obtained and compared.

7. Numerical behavior of deep beam

In this study, the effects of the orientation angle, width and arrangement of the CFRP sheets were investigated. The measured parameters include the ultimate strength and mid-span displacement of the concrete beams under study. In this study, the ultimate load is defined as the peak point on the load-displacement curve, representing the maximum load-carrying capacity of the beam. The failure load is defined as the point at which the beam's load-carrying capacity drops to 70% of the ultimate load after reaching the peak, indicating significant structural damage. Correspondingly, displacement at ultimate load refers to the mid-span deflection at the peak point, while displacement at failure refers to the mid-span deflection when the load drops to 70% of the ultimate value. These definitions are consistently applied throughout Table 2

7.1 Effect of the a/d ratio in un-strengthened models

Numerical analysis results in ABAQUS software showed that deep concrete beams under four-point loading primarily experience shear failure in the region between the support and the load application point. In control samples (without reinforcement), shear cracks propagated diagonally from the corner of the support towards the loading point, leading to sudden failure of the beam at loads close to the ultimate load. This type of failure was brittle and shear in nature, accompanied by a sudden drop in the load-displacement curve.

Numerical analysis from Figure 6 shows that the ultimate loads for unreinforced reference beams with shear span-to-depth ratios (a/d) of 0.95, 1.1, 1.2, and 1.35 are 390, 374, 367, and 352 kN, respectively. The corresponding mid-span displacements at these ultimate loads for the beams are 0.94, 1.26, 1.29, and 1.52 mm, respectively. It is also observed that as the a/d ratio (shear span to beam height) decreases, the beam's load-carrying capacity increases while the mid-span displacement decreases.

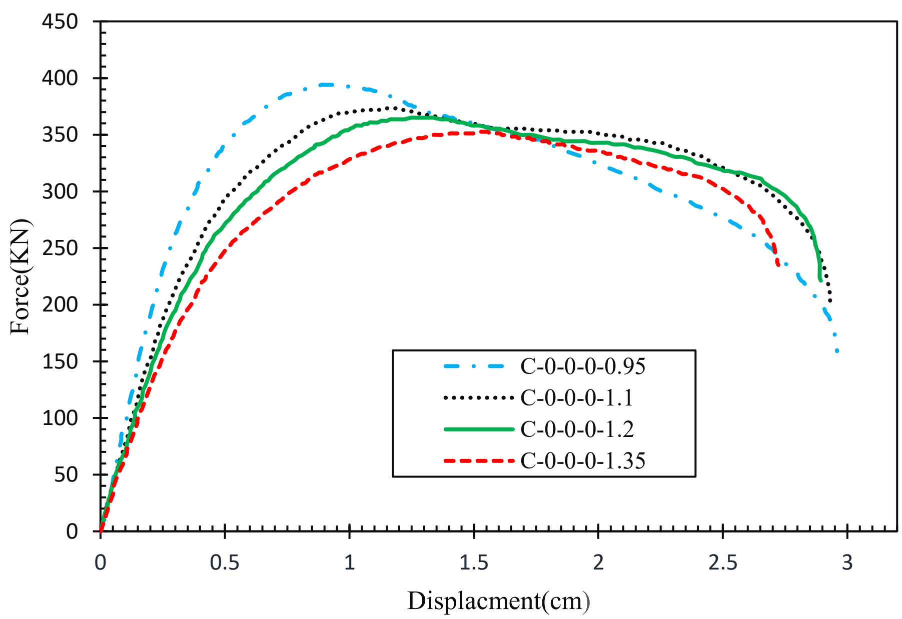

Fig. 6: Load-displacement diagram of beams without strengthening

In contrast, samples strengthened with CFRP sheets exhibited more ductile behavior. In these samples, CFRP sheets restrained the propagation of diagonal cracks, leading to more uniform stress distribution in the beam web and largely preventing shear stress concentrations in critical zones. As a result, ultimate failure in these beams occurred with larger deformations and greater ductility.

7.2 Effect of CFRP arrangement angle

7.2.1 Arrangement at 45 degrees

Figure 7 shows the load-displacement curves for CFRP-strengthened beams at a 45° angle with varying widths and different a/d ratios. The ultimate capacities for models C-1-45-18-0.95, C-1-45-18-1.1, C-1-45-24-1.2, and C-1-45-30-1.35 are 510, 440, 395, and 363 kN, respectively, representing ultimate load increases of 30.77%, 17.65%, 7.63%, and 3.1% compared to reference beams. As the a/d ratio decreases, shear contribution to overall behavior increases, shifting beam response from flexural to shear-dominated; CFRP use significantly enhanced ultimate load capacity across all ratios, though CFRP sheet width did not consistently increase capacity, with a/d ratio proving more influential.

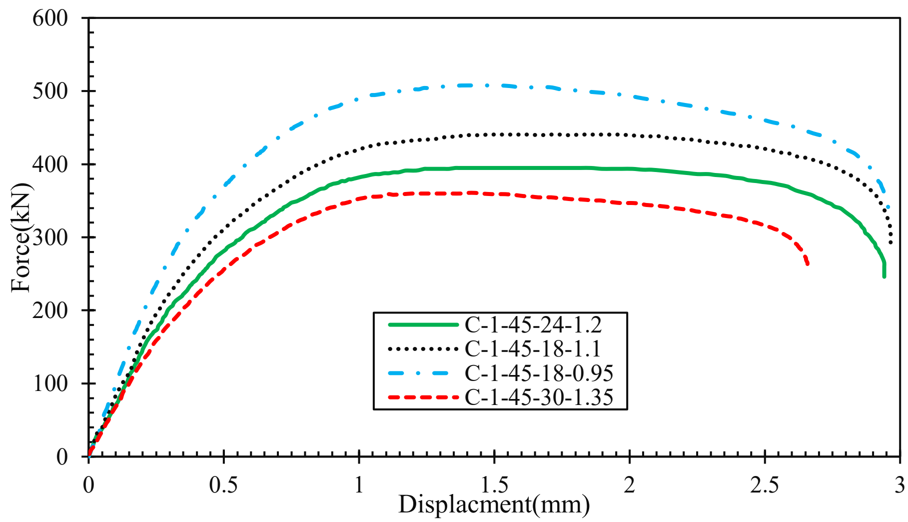

Fig. 7: CFRP sheet Arrangement at 45° angle with different widths

7.2.2 Arrangement at 135° angle

Figure 8 shows the load-displacement diagram for CFRP strips placed at a 135° angle. The ultimate capacities for models C-5-135-5-0.95, C-5-135-5-1.1, C-5-135-5-1.2, and C-5-135-5-1.35 are 586, 475, 421, and 368 kN, respectively. The ultimate load increases after strengthening compared to the control (unstrengthened) models are 50.26%, 27%, 14.71%, and 4.54%, respectively.

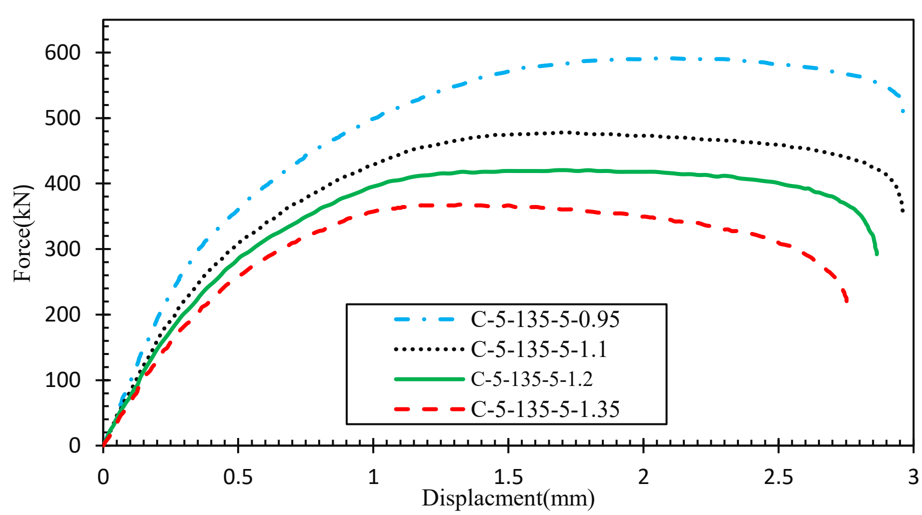

Fig. 8: CFRP sheet arrangement at 135° angle

The mid-span displacements for the above beams are 2.15, 1.63, 1.44, and 1.27 mm, respectively. The results indicate that as the a/d ratio decreases, the ultimate load increases while the mid-span displacement of the beam decreases.

7.2.3 Arrangement at 90° angle

Figure 9 shows the load-displacement diagram for CFRP strips placed at a 90° angle. The ultimate capacities for models C-5-90-5-0.95, C-5-90-5-1.1, C-5-90-5-1.1, and C-5-90-5-1.2 are 383, 368, 362, and 350 kN, respectively. Compared to reference models, this strengthened system shows no improvement in deep beam resistance because the fibers are not aligned with the crack paths, which typically form along the line between concentrated load points and supports.

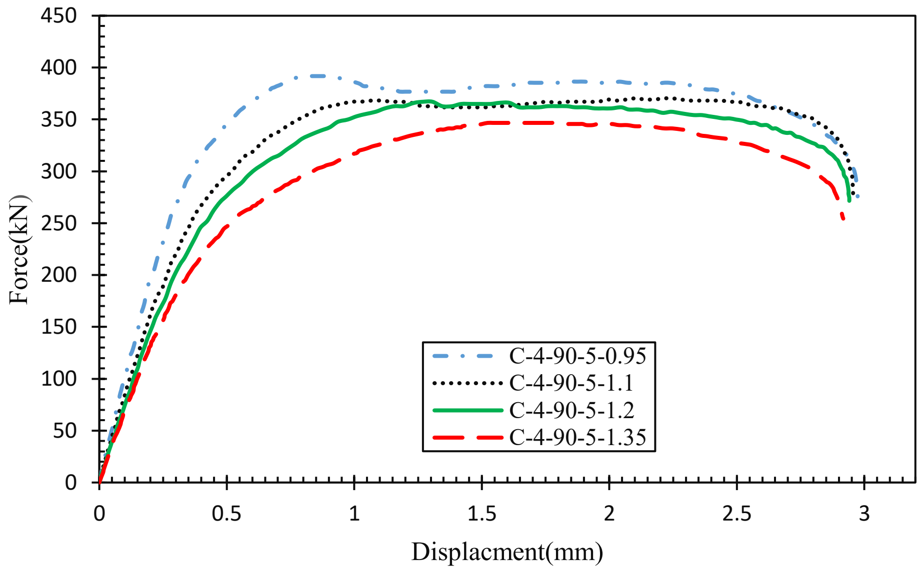

Fig. 9: CFRP sheet arrangement at 90° angle

The mid-span displacements for the above beams are 0.85, 0.98, 1.30, and 1.56 mm, respectively. As observed, the mid-span displacement of the beam increases with increasing a/d ratio.

7.2.4 Effect of CFRP sheet arrangement angle with constant a/d ratios.

In this section, the strengthened methods for models with identical dimensions using the approaches mentioned in Table 1 are examined. Figure 10 shows the load-displacement diagrams of the models.

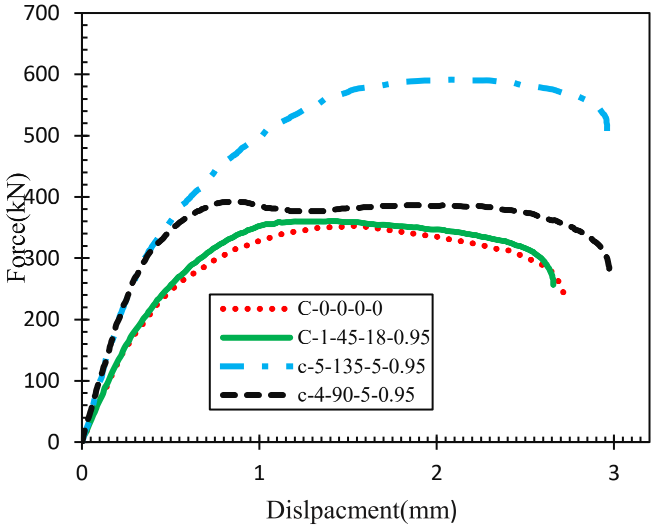

a: a/d=0.95:a

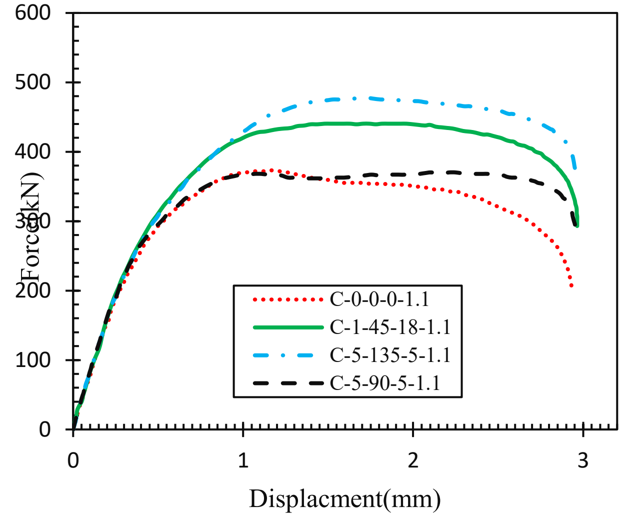

b: a/d=1.1

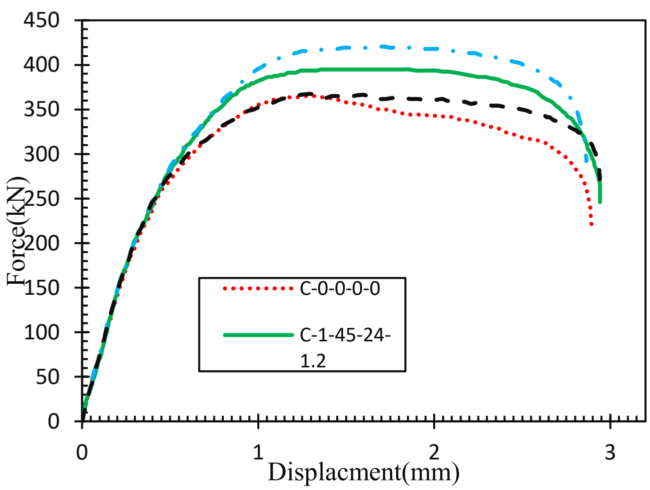

c: a/d=1.2

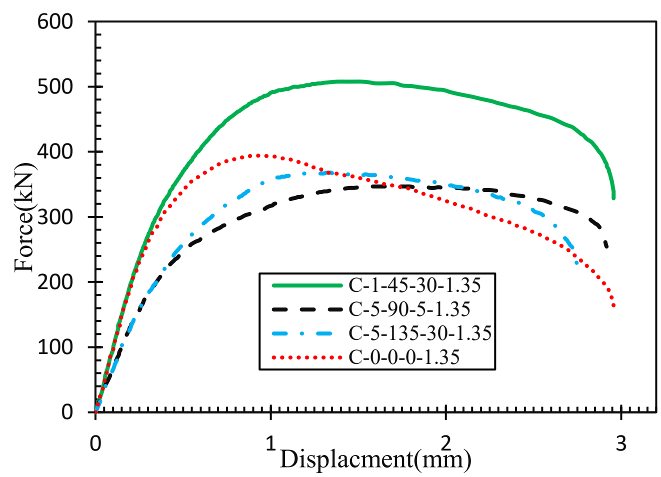

d: a/d=1.35

Fig. 10: Load-displacement different a/d and strengthened methods

Based on the diagrams in Figure 10, it is observed that for beams exhibiting shear behavior (i.e., those with lower a/d ratios), such as in Figures 10-a, 10-b, and 10-c, the best performance corresponds to sheets placed at a 135° angle. On average, the ultimate capacity increase in strengthened beams compared to control beams was reported as 45 to 55 percent, with the highest ultimate strength gain observed in the beam model with a/d = 0.95, while for a/d = 1.35, the CFRP effect was more limited. This confirms that CFRP effectiveness is greater in beams with dominant shear behavior. The numerical values and percentage increases in ultimate strength are presented in Table 3.

Table 3: Ultimate Strength Results of the Models

Model	a/d	ultimate load (KN)	Displacement in fracture (mm)(70% of ultimate load)	Displacement ultimate load (mm)	CFRP Contribution (KN)	Increasing capacity by strengthen *(%)*
C-0-0-0-0.95	0.95	390	0.94	2.97	-	-
C-0-0-0-1.1	1.1	374	1.26	2.94	-	-
C-0-0-0-1.2	1.2	367	1.29	2.93	-	-
C-0-0-0-1.35	1.35	352	1.52	2.78	-	-
C-1-45-18-0.95	0.95	510	1.47	2.97	120	30.77
C-1-45-18-0.1	1.1	440	1.85	2.97	66	17.65
C-1-45-24-1.2	1.2	395	1.90	2.96	28	7.63
C-1-45-30-1.35	1.35	363	1.31	2.71	11	3.1
C-5-135-5-0.95	0.95	586	2.15	2.98	196	50.26
C-5-135-5-1.1	1.1	475	1.63	2.96	101	27
C-5-135-5-1.2	1.2	421	1.44	2.91	54	14.71
C-5-135-5-1.35	1.35	368	1.27	2.83	16	4.54

Upon closer scrutiny of the ultimate stress contours in concrete and reinforcing steel against finite element predictions, the 135° CFRP laminate orientation demonstrates superior stress dispersion across all analyzed models. This configuration minimizes stress concentrations, enhancing overall structural performance under peak loading conditions.

Examination of Figures 11(a) through 11(g), depicting concrete tensile cracking damage and reinforcement stresses in beams, reveals that for the shear span-to-depth ratio (a/d = 0.95), no tensile cracking occurs along the line connecting the concentrated load to the support.

However, as the a/d ratio increases, beam cracking extends beyond the mid-span to the load-support connection line, causing premature failure and reduced ultimate load capacity in beams with higher a/d ratios under this strengthened scheme. For models C-5-135-5-0.95, C-5-135-5-1.1, C-5-135-5-1.2, and C-5-135-5-1.35, reinforcement stresses reach 250.4, 233.5, 231, and 208.1 MPa, respectively.

Comparison of stress contours demonstrates that higher a/d ratios result in lower peak reinforcement stresses, with fewer and shorter reinforcement segments reaching yield limits, indicating enhanced CFRP shear strengthened effectiveness. This behavior aligns with finite element predictions obtained using concrete damaged plasticity models for 30 MPa compressive strength concrete.

Table 4 shows the stiffness and ductility parameters for the unstrengthened models with CFRP sheets at an angle of 135 degrees. The results show that the reinforced models have higher initial stiffness. It is also observed that the ductility coefficient decreases with increasing the ratio a/d.

Table 4: Ductility and Stiffness Results of the Models

Model	a/d	yield load (KN)	Δ_Y(mm)	Δ_U(mm)	$k = \frac{\Delta_U}{\Delta_Y}$	$\mu = \frac{V_U}{\Delta_Y}$
C-0-0-0-0.95	0.95	276.9	0.46	2.63	601.96	5.72
C-0-0-0-1.1	1.1	262.7	0.38	2.77	691.31	7.28
C-0-0-0-1.1	1.2	306.45	0.41	2.68	747.43	6.53
C-0-0-0-1.35	1.35	329.4	0.35	2.11	941.14	6.03
C-5-135-5-0.95	0.95	500.24	0.59	2.96	847.86	5.02
C-5-135-5-1.1	1.1	425.6	0.61	2.95	697.70	4.84
C-5-135-5-1.2	1.2	389.82	0.6	2.82	649.70	4.7
C-5-135-5-1.35	1.35	315.67	0.53	2.59	595.60	4.89

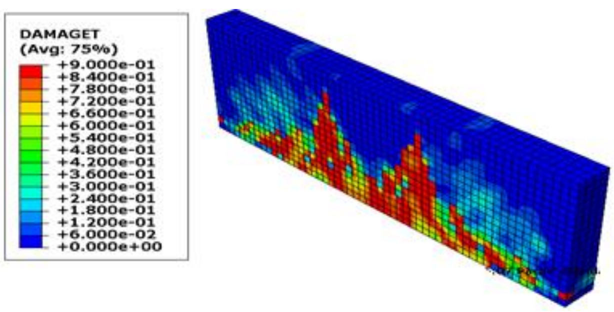

A: cracking stress *C-5-135-5-0.95*

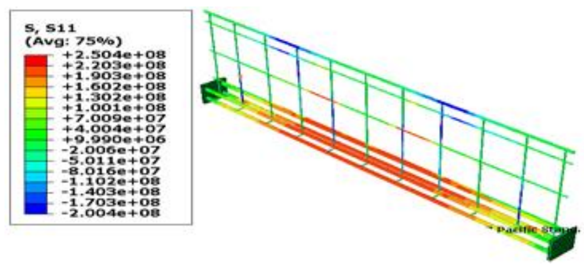

B:rebar stress *C-5-135-5-0.95*

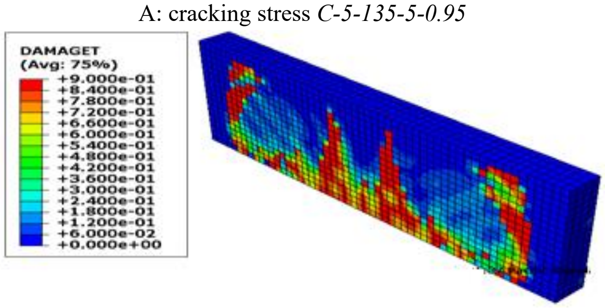

c: cracking stress *C-5-135-5-1.1*

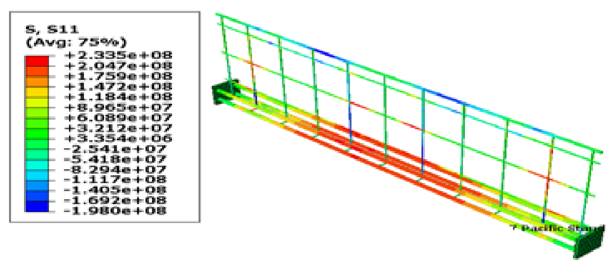

D:rebar stress *C-5-135-5-1.1*

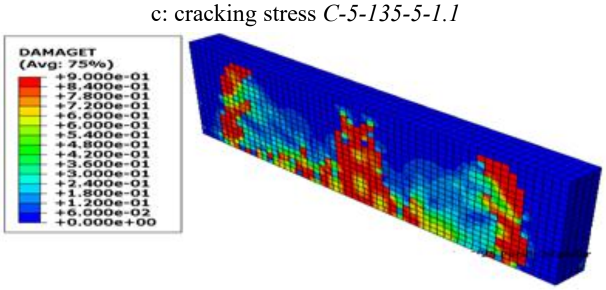

E: cracking stress *C-5-135-5-1.2*

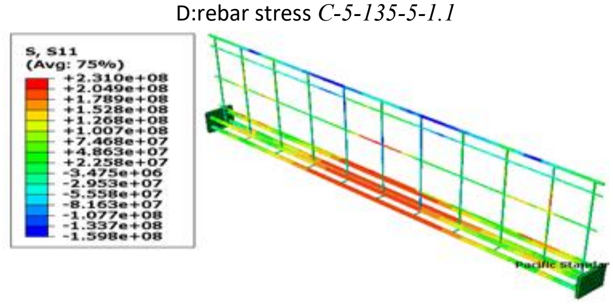

F:rebar stress *C-5-135-5-1.2*

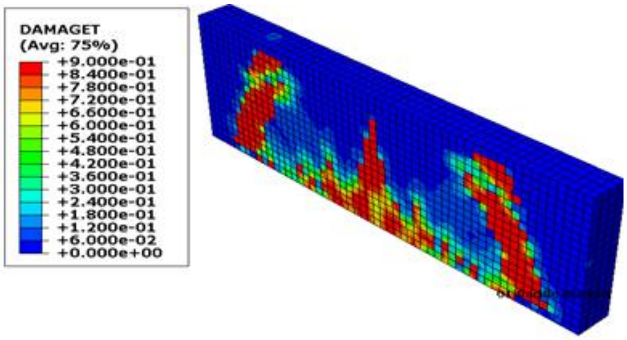

G: cracking stress *C-5-135-5-1.35*

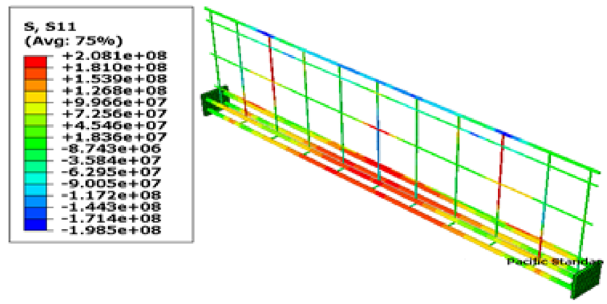

H: rebar stress *C-5-135-5-1.35*

Fig. 11: Stress contours in rebar and concrete for CFRP-strengthened models at 135° fiber orientation

8. Conclusions and future work

In this study, the effects of CFRP sheet orientation angle and configuration on the shear behavior and ultimate capacity of deep reinforced concrete beams were investigated. The variable parameter was the shear span-to-depth ratios (a/d), which were investigated using numerical modeling in the ABAQUS software. The obtained results are as follows:

- ***CFRP shear strengthened efficacy**: Beams* retrofitted with 135° CFRP sheets demonstrated up to 50% ultimate load enhancement for a/d = 0.95, validating finite element predictions using concrete damaged plasticity (f'c = 30 MPa) and Hashin failure criteria for composites.
- **Optimal CFRP fiber orientation:** 135° diagonal layout maximizes shear enhancement by aligning with diagonal tension crack trajectories, outperforming 90° vertical configurations that fail to intercept critical shear flow paths in deep beams.
- **a/d ratio sensitivity:** CFRP shear enhancement maximizes in deep beams (a/d = 0.95) with up to 50% ultimate capacity gain, decreasing progressively as beams transition to flexure-controlled failure at higher a/d ratios (1.1-1.35), per finite element parametric analysis.
- **Ductility improvement via stress redistribution**: C FRP laminate sheets retrofitting achieves uniform shear stress dispersion in beam webs, eliminating stress concentrations at load-support lines and transitioning failure modes from brittle shear to ductile mechanisms, as evidenced by reduced tensile damage contours in concrete damaged plasticity models.

Based on the findings, CFRP sheet shear strengthening of deep reinforced concrete beams, particularly with diagonal configurations in low a/d ratio geometries, constitutes an effective and practical method for enhancing ultimate capacity and structural ductility. Due to its low weight, high strength, and ease of application, this approach represents a suitable option for retrofitting concrete beams in bridges, buildings, and shear/earthquake-resistant structures.

To generalize the results to more realistic conditions and advance the research, the following are recommended:

1. Investigate additional parameters such as CFRP-concrete bond quality, rebar slip in concrete, boundary conditions, dynamic/fatigue effects, and asymmetric loading scenarios.
2. Conduct experimental tests alongside numerical simulations to validate the accuracy of numerical model results and verify the strengthened model.
3. Perform a comprehensive economic evaluation encompassing installation costs, long-term durability, and maintenance requirements to benchmark CFRP retrofit efficacy against traditional steel shear reinforcement.

Finally, it is important to acknowledge a key limitation of the present numerical study. All models assumed a perfect bond between the CFRP sheets and the concrete surface. This simplification ignores the possibility of interfacial debonding, which is a common failure mode in shear-strengthened RC deep beams, especially under dominant shear behavior (low a/d ratios). Consequently, the reported increases in ultimate capacity (e.g., up to 50%) should be interpreted as upper-bound estimates. For practical design applications, experimental validation or advanced interface modeling incorporating bond-slip behavior is strongly recommended.

References

[1] "A Simple Approach to Predict the Shear Capacity and Failure Mode of Fix-ended Reinforced Concrete Deep Beams based on Experimental Study," *Int. J. Eng.*, vol. 32, no. 4, Apr. 2019, doi: 10.5829/ije.2019.32.04a.03.

[2] A. Al-khreisat, M. Abdel-Jaber, and A. Ashteyat, "Shear Strengthening and Repairing of Reinforced Concrete Deep Beams Damaged by Heat Using NSM–CFRP Ropes," *Fibers*, vol. 11, no. 4, p. 35, Apr. 2023, doi: 10.3390/fib11040035.

[3] A. Abadel, "Shear strengthening of deficient RC deep beams using NSM FRP system: Experimental and numerical investigation".

[4] A. Kumar and R. Jangid, "Experimental and analytical study of shear strengthening of deep RC beams using externally bonded CFRP system," *Innov. Infrastruct. Solut.*, vol. 9, no. 7, p. 284, 2024.

[5] A. Arabzadeh and H. Karimizadeh, "Experimental study of RC deep beams with opening and FRP composites installed by means of EBR and EBROG methods," *Constr. Build. Mater.*, vol. 208, pp. 780–791, May 2019, doi: 10.1016/j.conbuildmat.2019.03.055.

[6] A. Kumari, S. S. Patel, and A. N. Nayak, "Shear Strengthening of RC Deep Beam Using Externally Bonded GFRP Fabrics," *J. Inst. Eng. India Ser. A*, vol. 99, no. 2, pp. 341–350, Jun. 2018, doi: 10.1007/s40030-018-0272-0.

[7] H. C. Akkaya, C. Aydemir, and G. Arslan, "An experimental research on reinforced concrete deep beams fully wrapped with fiber reinforced polymers against shear," *Case Stud. Constr. Mater.*, vol. 17, p. e01198, Dec. 2022, doi: 10.1016/j.cscm.2022.e01198.

[8] N. Al-Bayati, B. Muhammad, and S. Sadkhan, "Retrofitting of shear strength self-compacting reinforced concrete deep beams with FRP," *MATEC Web Conf.*, vol. 162, p. 04016, 2018, doi: 10.1051/matecconf/201816204016.

[9] S. Ma, J. Sun, and T. Xu, "Numerical Analysis of Shear Contribution of CFRP-Strengthened RC Beams by Different Bond-Slip Models," *Int. J. Concr. Struct. Mater.*, vol. 19, no. 1, p. 4, Jan. 2025, doi: 10.1186/s40069-024-00728-2.

[10] S. Ma, J. Sun, and T. Xu, "Numerical Analysis of Shear Contribution of CFRP-Strengthened RC Beams by Different Bond-Slip Models," *Int. J. Concr. Struct. Mater.*, vol. 19, no. 1, p. 4, Jan. 2025, doi: 10.1186/s40069-024-00728-2.

[11] Y.-L. Bai, J.-G. Dai, and J. G. Teng, "Buckling of steel reinforcing bars in FRP-confined RC columns: An experimental study," *Constr. Build. Mater.*, vol. 140, pp. 403–415, Jun. 2017, doi: 10.1016/j.conbuildmat.2017.02.149.

[12] H. K. Lee, S. H. Cheong, S. K. Ha, and C. G. Lee, "Behavior and performance of RC T-section deep beams externally strengthened in shear with CFRP sheets," *Compos. Struct.*, vol. 93, no. 2, pp. 911–922, Jan. 2011, doi: 10.1016/j.compstruct.2010.07.002.

[13] J. A. Bhat, "Effect of CFRP-Reinforcement variation on the strength parameters of different timber beams," *Mater. Today Proc.*, vol. 44, pp. 2785–2791, 2021, doi: 10.1016/j.matpr.2020.12.783.

[14] K. S. Ismail, M. Guadagnini, and K. Pilakoutas, "Strut-and-Tie Modeling of Reinforced Concrete Deep Beams," *J. Struct. Eng.*, vol. 144, no. 2, p. 04017216, Feb. 2018, doi: 10.1061/(ASCE)ST.1943-541X.0001974.

[15] P. D. Zararis, "Shear Compression Failure in Reinforced Concrete Deep Beams," *J. Struct. Eng.*, vol. 129, no. 4, pp. 544–553, Apr. 2003, doi: 10.1061/(ASCE)0733-9445(2003)129:4(544).

[16] M. A. Javed, M. Irfan, S. Khalid, Y. Chen, and S. Ahmed, "An experimental study on the shear strengthening of reinforced concrete deep beams with carbon fiber reinforced polymers," *KSCE J. Civ. Eng.*, vol. 20, no. 7, pp. 2802–2810, Nov. 2016, doi: 10.1007/s12205-016-0739-3.

[17] M. I. Kabir, M. Subhani, R. Shrestha, and B. Samali, "Experimental and theoretical analysis of severely damaged concrete beams strengthened with CFRP," *Constr. Build. Mater.*, vol. 178, pp. 161–174, Jul. 2018, doi: 10.1016/j.conbuildmat.2018.05.038.

[18] M. F. Jassim, Y. J. Lafta, and H. S. Malik, "Shear Behavior of Reinforced Concrete Beams with Different Arrangements of Externally Bonded Carbon Fiber-Reinforced Polymer," *J. Eng.*, vol. 2023, pp. 1–9, Jul. 2023, doi: 10.1155/2023/1465410.

[19] A. Szewczak, "Influence of Epoxy Glue Modification on the Adhesion of CFRP Tapes to Concrete Surface," *Materials*, vol. 14, no. 21, p. 6339, Oct. 2021, doi: 10.3390/ma14216339.

[20] K. Śliwa-Wieczorek, K. A. Ostrowski, J. Jaskowska-Lemańska, and A. Karolak, "The Influence of CFRP Sheets on the Load-Bearing Capacity of the Glued Laminated Timber Beams under Bending Test," *Materials*, vol. 14, no. 14, p. 4019, Jul. 2021, doi: 10.3390/ma14144019.

[21] M.-S. Jo, H.-G. Kim, D.-H. Kim, S.-A. Lim, H. Kong, and K.-H. Kim, "Evaluation of Behavior Characteristics of Reinforced Concrete Beam Shear Strengthening with Different FRCMs," *Buildings*, vol. 14, no. 12, p. 3949, Dec. 2024, doi: 10.3390/buildings14123949.

[22] F. Zhang and L. Gao, "Finite Element Model for Analysis of the Spatial Interfacial Debonding of FRP from Concrete," *Adv. Compos. Lett.*, vol. 26, no. 3, pp. 89–100, doi: https://doi.org/10.1177/096369351702600305.

[23] S. S. Chiriki and G. S. Harsha, "Finite element analysis of RC deep beams strengthened with I-section and truss reinforcement," *Mater. Today Proc.*, vol. 33, pp. 156–161, 2020, doi: 10.1016/j.matpr.2020.03.579.

[24] M. Ghalla, G. Elsamak, A. El-Zohairy, O. Youssf, S. Khairy, and A. Badr el-din, "Experimental investigation on the structural performance of strengthened reinforced concrete deep beams using steel-based and SHCC techniques," in *Structures*, Elsevier, 2026, p. 111074.

[25] G. Priyasri, S. Gollapalli, P. J. Varma, S. K. Muniasamy, P. Praveena, and S. Annam, "Fusion-Based Data-Driven Strength Prediction of Bamboo Fiber-Reinforced Concrete for Sustainable Construction," 2026.

[26] M. Samhan, M. Shhabat, M. Abdel-Jaber, and A. Ashteyat, "Shear strengthening and rehabilitation of heat-damaged RC deep beams with openings using CFRP: experimental and numerical study," *J. Asian Archit. Build. Eng.*, pp. 1–23, 2026.

[27] "Defining parameters for concrete damage plasticity model," *Chall. J. Struct. Mech.*, 2015, doi: 10.20528/cjsmec.2015.07.023.

[28] M. Shabanlou, M. Mofid, and A. Tavakoli, "Experimental and Numerical Study on the Behavior of Reinforced Concrete Deep Beams with Normal-Strength and High-Strength Concrete After Being Exposed to Fire," *Arab. J. Sci. Eng.*, vol. 49, no. 10, pp. 13457–13476, Oct. 2024, doi: 10.1007/s13369-023-08676-x.